Engineered Science
DOI: https://dx.doi.org/10.30919/es1135

Investigation into Effect of Magnetic Moments to Swimming Behavior and Performance of the Soft Milli-Film Robots

Xiuzhen Tang[#] and Laliphat Manamanchaiyaporn[#,*]

Abstract

For years, soft swimming milli-robots have been developed by various techniques to fulfil medical therapy and treatment. Real-time remote controllability, small size, soft interface, and non- toxicity are critical requirements for them to cope with blind, unstructured, and fluidic conditions inside life. Theoretically, the magnetic response of the robot to actuation relies on magnetic moments that behave as a vector, and they consist of orientation and strength. In soft swimming robotics, they are employed as a motor-less mechanism for the swimming through a deformable structure with high degrees of freedom provided by compliance with minimal control of a magnetic field. Here, this work investigates how both aspects impact the swimming behavior and performance of the soft-structured milli-robots. Elastomer and NdFeB-microparticles are utilized to fabricate three robots with distinguishing aspects of magnetic moments (uniform/non-uniform orientation coupled with uniform/non-uniform strength). Under the same control parameters and testing conditions, the experimental results interestingly report that each aspect provides a mechanism and benefit of swimming performance for the robots differently. Non-uniform orientation mainly influences the pattern of body transformation, but non-uniform strength relates to how fast the body transforms. The robot with the aspect of both non-uniform orientation and strength is the best swimmer. If the scale of the robot is down in micrometers, non-uniform strength is highly recommended to define the swimming mechanism. These findings are useful for designing an individual robot to operate in life by choosing a proper aspect to fit medical tasks significantly.

Keywords: Magnetic soft actuator; Soft robotics; Magnetic manipulation.
Received: 19 November 2023; Revised: 12 March 2024; Accepted: 21 April 2024.
Article type: Research article.

1. Introduction

Living body insides is a fantastic and complex system that consists of the circulation of diverse biological fluids and unstructured environments of organs. Untethered miniature robots with a less-than-millimeter size have been promising to access biological regions and perform medical tasks (*e.g.*, targeted drug delivery, biopsy, minimally invasive treatments).[1] However, design and fabrication process are crucial to make robots meet the potential standard for motion mechanism, function, further applications, and environmental interactions the robots are operated. Due to the size in sub-millimeter or less, neither a battery nor the mechanism is tiny enough to set up inside the robot's structure. Consequently, a method to power the robot for locomotion and functional trigger must rely on remotely wireless techniques. Active elements and chemical substances are then embedded in their body to respond to external power sources (*e.g.*, chemical reaction, light, magnetic field), and later converts them into a motor-less mechanism. Some types of robots received light-emission pulses to switch between its elongating and shortening structure for creeping mobility. Another employed chemical reaction to surrounding medium for propulsion (*i.e.*, urine). Another embedded with magnetic elements were active in a magnetic field for locomotion.

Currently, the use of magnetic fields has broadly proved no harm to human tissue (*e.g.*, MRI clinical imaging). It is then one of the most selective sources to remotely power small-scaled robots. Both torque and force exerted on the robots can

Center of Excellence in Creative Engineering Design and Development, Research Unit in Multi- Scale Robotics, Thammasat School of Engineering, Faculty of Engineering, Thammasat University, 12120, Thailand.
[#] These authors contributed to this work equally.
**Email:* mlalipha@engr.tu.ac.th (L. Manamanchaiyaporn)

navigate them to arbitrary positions by the mean of the controllable magnetic field generated by the Electromagnetic Actuation System EMA) which is specifically designed in diverse configurations and integrated with a variety of control techniques to serve a potential control and performance (*e.g.* Helmholtz coil, Maxwell, visual servoing based control, *etc*.).[2] As mentioned, active elements can make the robots active, and in case of magnetic elements embedded in the robots' structure, they define the magnetic property of the robots. This is called magnetization which behaves as a motor-less mechanism, and enables magnetic force and torque to drive the robots for effective motions along the dynamic magnetic field.[3]

As mentioned, a small-scaled robot can contribute to medical outcomes promisingly, but inside a life, biological environments are viscous, uneven, unstructured, and difficult to any matter able to perform physical actions and movements. The robots then employed an asymmetric movement of microorganisms as a key success to achieving swimming in a biological fluid (*e.g.* beating of flagella, waving of cilia, helical propulsion).[4,5] However, most swimming robots were structured with solid materials that were not safe for interaction with nearby tissues, organs, *etc*. The transition from a hard structure to a soft structure is consequently alternative interest through the material fabrication process of flexible materials embedded with active elements, eventually leading to a new concept of robots called soft swimming robots.[6] The integration of magnetic microparticles into a deformable structure enables structural controllability under magnetic actuation.[7,8] Naturally, magnetic moments or magnetization embedded in all specimens of a robot's soft structure align with the actuating magnetic field, and simultaneously induces the soft structure, leading to on-demand structural deformation. When the deformation is controllable and proceeds continuously under a magnetic field, the robot's movement is asymmetric, resulting in locomotion significantly. These robots utilize high degrees of freedom-based deformation provided by magnetic compliance with minimal control of the magnetic field.[9] This aspect does not only benefit the robots, but it also allows magnetic-based medical tools and devices more dexterous in various types of biomedical applications (*e.g.* compliant-soft medical tools, flexible wearable devices).[10] Moreover, an advantage of the soft structure is a soft interface without harmfulness to where the robots pass through.[11] Adding more matters (*e.g.*, drug molecules, chemical nanoparticles) into the soft structure was available during the fabrication process to fulfil further biomedical applications, such as drug delivery, biopsy, detoxification.[12-16]

In previous research, the soft robots employed anisotropic magnetization to generate body deformation based on a continuous alignment of the heterogeneous orientation of magnetic moments with the dynamic magnetic field. The deformation degree of each specimen is equal over the robot structure because the distribution of magnetic moments in those specimens is homogeneous over the whole soft structure, resulting in uniform magnetic strength. However, the property of magnetic moments embedded in the soft structure still remains a challenge in core details. That is, magnetic moment typically comprises orientation and strength, and what if either and both of them is not uniform across the whole soft structure of the robot. Moreover, currently, the heterogeneous orientation is only employed to characterize how the robot transforms its body, and the result is obviously feasible, but programming the orientation of magnetic moments by means of a physical magnetizing process is not simple and less precise for the robot with a scale less than one millimeter. Thus, it would be better to have another alternative solution to compensate such that constraint. In this work, the effect of magnetic orientation and strength in the deformable structure of the soft swimming milli-robot is investigated in terms of lateral undulation-based swimming behavior and performance under the same control parameters. Three types of soft milli-robots are fabricated for swimming experiments; the I robot: uniform magnetic strength and non-uniform magnetic orientation, II: non-uniform magnetic strength and uniform magnetic orientation, and III: non-uniform magnetic strength and orientation. The outcome will provide pros and cons for the robot design to fit for specific applications, to cope with unwanted situations, and to enhance the swimming potential of the robots in biological fluid for treatment and therapy.

Methods and materials are detailed in the next section. Next, experiments are conducted to test the performance in swimming of the robots in a fluid under the change in controlled parameters. Finally, the conclusion is issued.

2. Experimental section

2.1 Conceptual design

Since the size of an object that moves in media is in millimeters or less, the inertia term dominates the viscous term, resulting in a condition of low Reynold number ($Re < 1$). Purcell stated that one of feasible motion patterns under low Reynold number was an asymmetric body deformation under time reversal.[17] As mentioned, a soft interface is one of critical requirements for the robot to avoid physical damage to nearby tissues and organs during operating insides. A suitable property of a main material to fabricate a robot to serve the demands of both asymmetric deformation and the soft

interface is about flexibility, elasticity and compliance. Consequently, firstly, the base material is liquid silicone rubber (LSR) because it can be fabricated into desired shapes according to applications. Secondly, it still provides a food and medical grade. Thirdly, it provides a soft interface and deformable structure compliant with the external stimuli. However, since the robot is scaled in millimeters or less, neither the battery nor the mechanism is currently small enough to set up inside the robot's structure. To remotely control the robot, active elements to receive a wireless power from an external source are important. Another base material, NdFeB magnetic microparticles, is chosen to embed inside the LSR structure to respond to a magnetic actuation. Since the mixture of both NdFeB microparticles and LSR is excited by the magnetic field, each microparticle starts aligning with the magnetic direction, and simultaneously induces each soft specimen of the structure to transform into a shape corresponding to the pattern of magnetic moments embedded within the structure. Thus, the NdFeB@LSR structure leads to the controllable-deformable property upon a demand under a magnetic field. Since the magnetic field is dynamic, the body deformation is ceaseless. This concept can be applied as a motor-less mechanism for the soft robots remotely powered by the magnetic field to serve as a medical device significantly. Based on the theoretical modeling of magnetism,[18] one single magnetic moment or a magnetic dipole within a magnetic material is a vector that consists of magnitude and direction. By the detail, either or both of them can affect the magnetic property of the object. Thus, magnetic moments in a soft milli-robot is expressed by

$$\vec{m} = \iiint M\, dV = \iiint M\, dA dl \quad (1)$$

where A, l are a cross-sectional area and length of the robot structure, respectively. M is magnetization as a vector quantity of magnetized magnetic moment in a robot volume V. In Fig. 1a, magnetic moments in all small specimens of a soft rectangular shape with thickness represented by upward arrows clearly depict uniform magnetic orientation. According to the Eq. (1), if considering a cross-section area of the robot's rectangular shape across the length which is symmetric, the quantity of magnetic moments is equal. That is, when cutting the rectangle robot into pieces along length, their cross-sectional area all remains same, resulting in uniform magnetic strength.

On the other hand, in Fig. 1b, magnetic moments in each specimen of the soft triangular body represented by upward arrows clearly depict uniform magnetic orientation, but when cutting it to pieces across the body length, unlike the rectangular body, quantity of magnetic moments in each cross-sectional area is unequal all over the length. It seems a larger area contains a higher quantity, resulting in non-uniform magnetic strength. The larger specimen will have a stronger magnetic strength. Thus, for the triangular body, magnetic strength decreases along the body length, and the Eq. (1) is rewritten to

$$\vec{m}(x) = \iiint M\,(x)\, dV(x) = \iiint M\, dA\,(x) dl \quad (2)$$

The Eq. (2) expresses that at a position x of the length, l, magnetic moments are a function of a cross-sectional area. If the area size is all unequal over the length, magnetic strength is non-uniform over the body. Therefore, to investigate the effect of magnetic moments, there are three possible approaches to shuffle the magnetic properties of the soft swimming milli-robots, which are; the I robot has uniform magnetic strength and non-uniform magnetic orientation, the II robot has non-uniform magnetic strength and uniform magnetic orientation, and the III robot has non-uniform magnetic strength and orientation.

2.2 Fabrication

In order to couple both orientation and strength to specify magnetic property of the soft structure, three possible solutions are both uniform magnetic orientation and strength, uniform magnetic orientation coupled with non-uniform magnetic strength, and vice-versa. As mentioned, three soft milli-robots are fabricated to have distinguished magnetic properties through the existence of magnetic moments in the structure. The main materials are listed in Table 1. In Figs. 2a-2b, the robot fabrication starts with mixing LSR with NdFeB

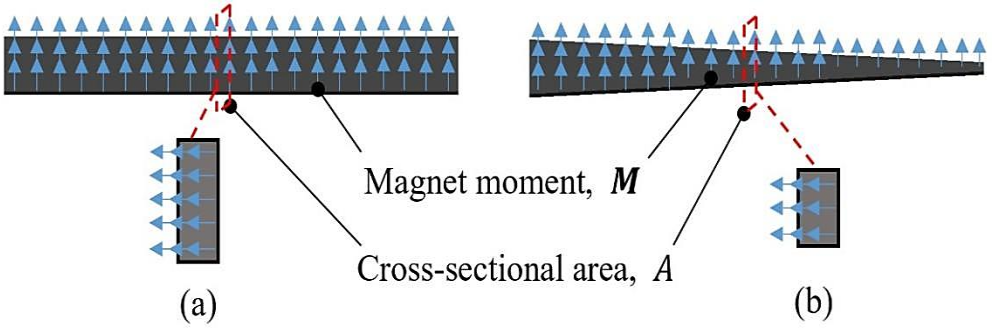

Fig. 1 The different magnetic property of magnetic-soft structure between previous works and this work. (a) uniform distribution of magnetic moments, (b) non-uniform distribution of magnetic moments.

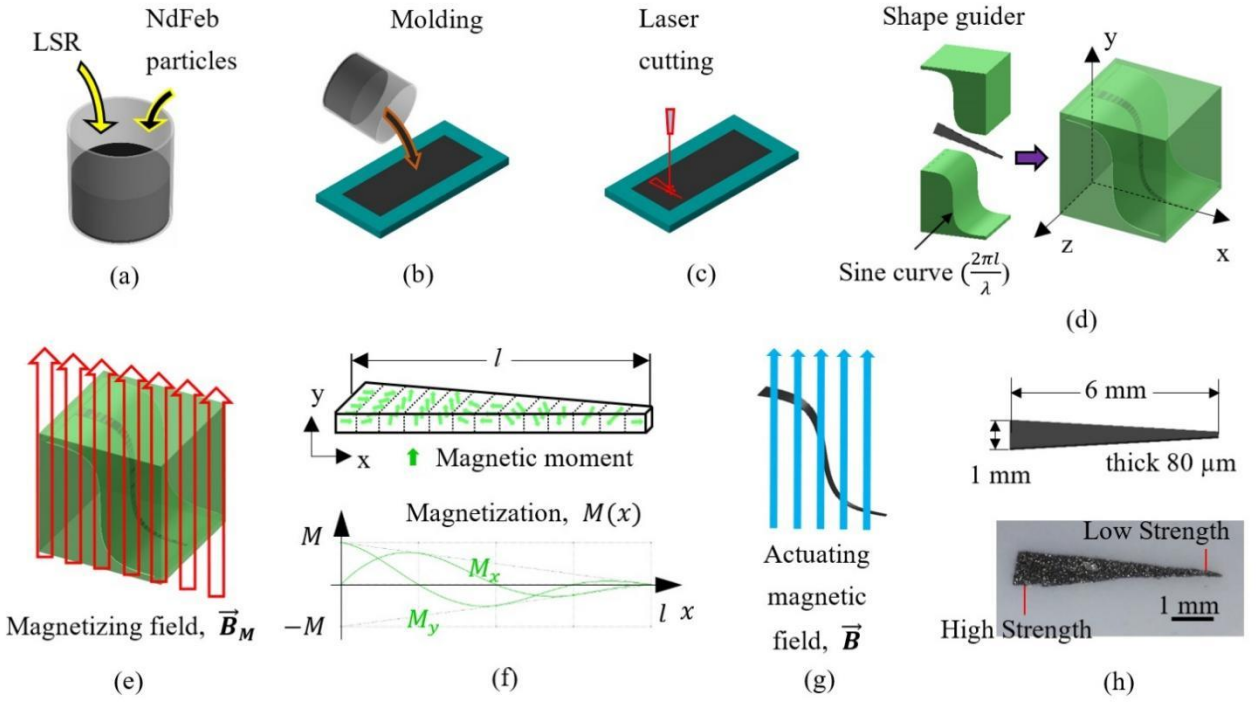

Fig. 2 Example of fabricating the III robot. (a) Liquid silicone substances and NdFeb particles with 1:1 of mixing ratio. (b) molding on the stainless-steel plate, then subjects it to heat curing. (c) cutting into a triangular shape. (d) inserting into the sinusoidal-surface shape guider. (e) 700 mT of uniform magnetizing magnetic field. (f) magnetization profile of the film robot: (upper) magnetic orientation. (lower) magnetic strength decreases by increasing the body length. (g) the robot responding to the actuating magnetic field. (h) (upper) dimension of the triangular body: 1 mm × 6 mm × 80 µm. (lower) the fabricated robot.

microparticles by the 1:1 mass ratio. Later, pour the slurry into a stainless-steel mold with an 80 µm cavity to form a 3D-magnetic soft sheet with 80 µm thickness, and then curing the mold at 250 ºC about 8-10 minutes to turn slurry into a solid sheet. In fact, the manufacturer suggests curing temperature of LSR about 200-220 °C, but it is found that at the 220 °C, the mixture needs at least 17 mins to complete curing. Consequently, the mixture is further investigated three times by increasing the curing temperature every 5 °C from 220 °C to 270 °C. The 250 °C is the most appropriate temperature due to having the shortest range of curing time. Next, at 250 °C, it is figured out that 8-10 minutes is the proper curing time. In less than 8 minutes, the mixture is partially turned into a solid. After more than 10 minutes, the mixture is swelled and permanently deformed. The curing temperature and time are reported in Table 2.

To define the magnetic property (strength and orientation of magnetic moments) of the sheet, there are two processes.

Table 1. Raw materials and tools.

Material	Property	Function
Liquid silicone rubber (LSR)	Density: 1.13 g/cm^3, Young modulus: 300 kPa, temperature resistance: -50 to 250ºC, tensile strength: 1.5 MPa, elongation at break: 700%	Base material to form a soft structure
NdFeB (Neodymium) magnetic Microparticles	Particle size: 4 µm to 40 µm, density: 7.57 g/cm^3, Remanence: 720-760 mT, coercivity: 360-480 A/m, magnetic energy: 80 to 98 kJ/m^3	Active elements; base material to respond to magnetic actuation
A stainless-iron plate	30 mm × 100 mm with 80 µm±10 µm cavity	A mold for the mixture (magnetic slurry) to form a magnetic-soft sheet
A shape guider	3D-printed part (PLA: Polylactic Acid) with sinusoidal profile* (sin($2\pi l/\lambda$) at the inner surface	To define constraint a magnetic-soft sheet before applying a magnetizing magnetic field to specific magnetic orientation of magnetic moments

* Profile to specify orientation of magnetic moments can be adjusted to any form.

Table 2. Investigations of curing temperature and time.

Temperature (°C)	220	225	230	235	240	245	250	255	260	265	270
Curing time (minutes)	>17	15-19	14-17	12-14	10-15	9-11	8-10	7-10	6-9	5-7	<5

Note that the temperature at 250 °C is the most appropriate because of the shortest range of curing time. Although the temperature more than 250 °C reports much more shorter curing time, it is found out that the mixture swells in some positions. All samples are tested Young's Modulus, and the results are almost similar.

Firstly, to define magnetic strength, in Fig. 2c, as expressed in the Eq. (2), magnetic moments are directly proportional to the size of the cross-sectional area of the robot. That is, the shape of the robot directly affects the magnetic strength of the robot. Consequently, the II and III robots are cut into a triangular shape to have non-uniform magnetic strength all over the body, but the I robot is cut into a rectangular shape to provide uniform magnetic strength. Secondly, to define magnetic orientation, in Figs. 2e-2h, the triangular and rectangular sheets are subjected to the 700-mT magnetizing magnetic field, $\vec{B}_M$. The I and III robots are formed as a wave in the shape guider, so the overall orientations of magnetic moments result in a waveform called a sine profile. For the II robot, the sheet is placed with the surface perpendicular to the direction of the magnetizing magnetic field, so the orientation of magnetic moments all points to the same direction. Specifications and properties of those three robots are detailed in Table 3.

Since the soft milli-robot is embedded with magnetic microparticles, the magnetic field can align magnetic moments, $\vec{m}$ to induce the soft structure to deform along the direction of the magnetic field. This concept is called a motor-less mechanism to drive the robot to swim in fluid compliant with a magnetic field.The Electromagnetic Actuation System in Fig. 3 can generate three-dimensional magnetic field, $\vec{B}$ expressed by

Table 3. Three types of soft swimming milli-robots.

Type	Width (w) Length (l) Thick (h)	Shape	Profile of magnetic orientation*	Magnetic strength**	Magnetic response
I	1 mm 6 mm 80 μm	Rectangular	Sine – Non-uniform	Uniform	
II	1 mm 6 mm 80 μm	Triangular	Transverse – Uniform	Non-uniform	
III	1 mm 6 mm 80 μm	Triangular	Sine – non-uniform	Non-uniform	

* A group of arrows depicts the direction of magnetic moments, and its number refers to magnetic strength in the robot's structure.
** A graph shows the relation of magnetic strength and magnetic orientation of magnetic moments as a function of the body length.

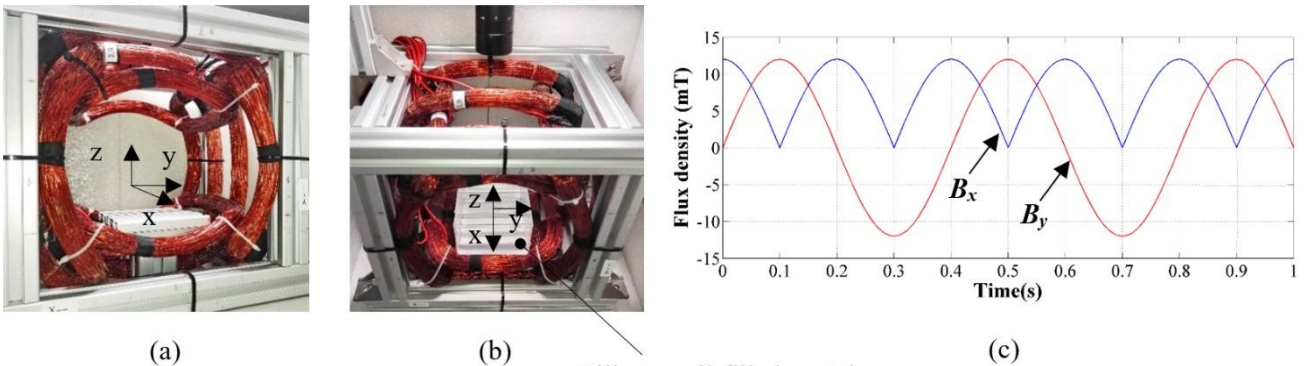

Fig. 3 Electromagnetic Actuation System. (a) homogeneous magnetic field is available across the large bore. (b) a silicone-filled container as a test reservoir of the robot inserted into the bore. (c) Actuation of oscillation signal based on the supposition of the x- and y-magnetic field, B_x and B_y, with 2.5 Hz.

$$\vec{B}= [B_x \quad B_y \quad B_z] \tag{3}$$

Once the robot is under magnetic field, magnetic torque, $\vec{T}$ and force, $\vec{F}$, are exerted to the robot, which is expressed by

$$\vec{F}(x) = \vec{m}(x).\nabla\vec{B} \tag{4}$$

$$\vec{T}(x) = \vec{m}(x).\vec{B} \tag{5}$$

In this work, the oscillating magnetic field is applied to exert a planar continuous torque on the robot to deform its structure, leading to the body wave propagation or lateral undulation-liked swimming. The oscillating magnetic field is a product of the resultant magnetic field caused by the superposition of the x- and y-direction magnetic field, B_x and B_y, which oscillates with frequency, f (Hz: cycle number in a second). According to the sample signal with 2.5 Hz frequency in Fig. 3c, the Eq. (3) is rewritten into

$$\vec{\boldsymbol{B}}(t) = B[|\cos(2\pi ft)| \quad \sin(2\pi ft) \quad 0]^T \tag{6}$$

Frequency and magnitude of the oscillating magnetic field in the Eq. (6) are adjustable by varying magnitude and direction of the electric input current supplied to each electromagnetic coil.

2.3 Modeling of deformable structure

Regarding the soft structure of robots, Euler-Bernoulli beam theory is adopted to determine the local body deformation caused by magnetic field, depicted in Fig. 4. Once magnetic torque, T, as bending moment, M_b, is exerted to the robot, expressed by

$$\boldsymbol{T}(x) = M_b = -EI\frac{\partial^3\theta}{\partial x^3} \tag{7}$$

where E is Young modulus of the robot (Pa), θ is bending angle defined by deformation degree over length estimated by $\theta = \frac{dy}{dx}$, and I is area moment of inertia (m^4) which is a function of the thickness, h, and width, w. When the body of robot is long, l, the area moment of inertial at each local body becomes a function of the unit length, x, of the full length, l, expressed by

$$I(x) = \frac{h^2hw}{12} = \frac{h^2A}{12} \tag{8}$$

where A is the cross-sectional area at the x position of the body length l. Substituting the Eq. (5) and the Eq. (8) in the Eq. (7), so

$$\left(\vec{\boldsymbol{m}}(t) \times \vec{\boldsymbol{B}}\right) = -E\frac{h^2A}{12}\frac{\partial^3 y}{\partial x^3} \tag{9}$$

$$y(x) = -\iiint \frac{12}{h^2EA}\left(\vec{\boldsymbol{m}}(x) \times \vec{\boldsymbol{B}}\right)\partial x^3 \tag{10}$$

As mentioned, considering that the whole body of the robot consists of many magnetic domains. Magnetic moments, $\vec{m}$, at a specimen or a local is a function of magnetization and cross-sectional area. The Eq. (10) expresses that deformation of a specimen at the position x of the body length depends on magnitude and direction of magnetic moments significantly. Differentiating the Eq. (10) over time to obtain swimming velocity, $\vec{U}$, at that local, is expressed by

$$\vec{\boldsymbol{U}}(x) = -\frac{3fBM\lambda^3}{\pi^2h^2E}\left[Sin\left(\frac{2\pi x}{\lambda} - 2\pi xft\right)\right]$$

$$\text{and } \vec{\boldsymbol{U}}(x) = +\frac{3fBM\lambda^3}{\pi^2h^2E}\left[Sin\left(\frac{2\pi x}{\lambda} + 2\pi xft\right)\right] \tag{11}$$

where f, B, M, λ, E, t is the oscillating frequency, magnetic field, magnetization, body wavelength, Young modulus of material, oscillating time respectively. Positive and negative sign express the deformation direction of a specimen of the body. From the Eq. (11), in short, the swimming velocity, $\vec{\boldsymbol{U}}$, is proportional to magnitude and direction of magnetic moment which is a function of magnetization, $\boldsymbol{M}$, at that specimen.

3. Results and discussion

As mentioned, the soft milli-robots in this work employ the asymmetric body deformation to swim in the fluid under the controllable magnetic field. Three robots are experimentally investigated in terms of swimming behavior and performance. Experiments are set up under the same parameters and conditions (*e.g.*, magnetic field, frequency, workspace). Three types of robots are all fabricated from the same mixture, but in the post-fabrication, each robot is cut differently to specify magnetic strength through the number of magnetic moments that relate to the robot's shape. They are subjected to the magnetizing process to program the orientation of magnetic moments. A tank that contains silicone oil to simulate the viscosity of a biological fluid is inserted into the bore of the Electromagnetic Actuation System to stand for experiments,

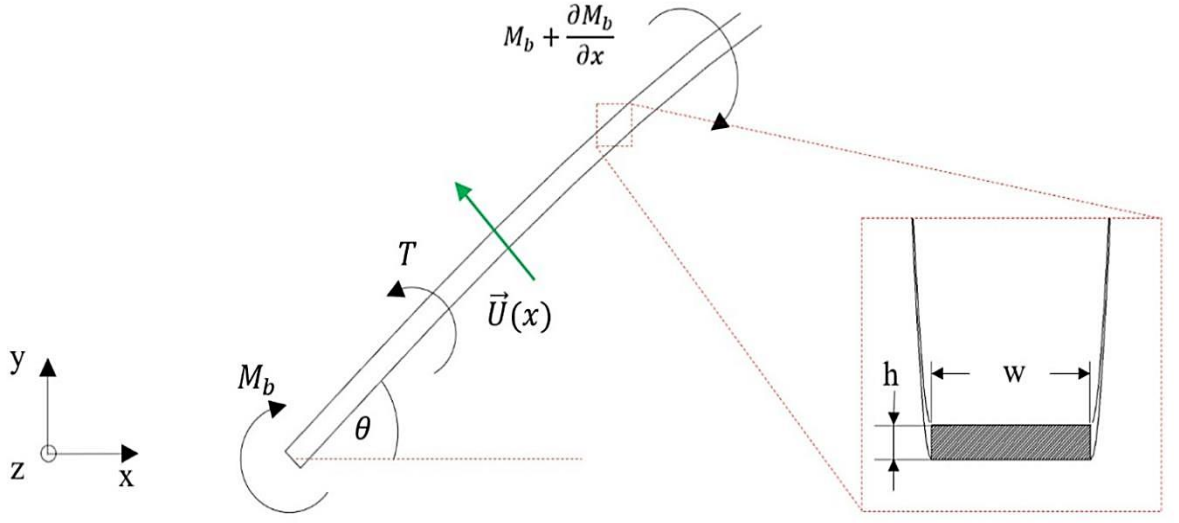

Fig. 4 Physical interpretation of a deformable structure. When magnetic torque is exerted to deform a soft robot long, l, a magnetic specimen of the body at the position x, with thickness, h, and width, w, is bent with deformation degree with angle, θ, and fast degree with velocity, $\vec{U}(x)$.

as depicted in Fig. 3b. Oscillating magnetic field is generated with three magnitudes (5, 10, 15 mT) and fifteen frequencies (1 to 15 Hz) to manipulate three types of the soft milli-robot. Quantitative evaluation is performed to collect swimming data of three robots. Each robot is experimented with three times to swim along the 10-cm distance within the testing reservoir under all input parameters (*i.e.*, magnetic field strength, frequency). As mentioned, the electromagnetic actuation system is mounted with the camera on the top. Visual servoing technique via a custom control GUI is applied to capture the swimming robots along a counting time during experiments. Finally, swimming velocity is calculated by the ratio of the swimming distance to time.

3.1 Magnetic behavior of the I robot

The property of the I robot consists of uniform magnetic strength due to a rectangular film shape (1 mm × 6 mm × 80 μm), and non-uniform magnetic orientation due to having a sine profile magnetization, detailed in Table 3. Thus, its magnetic property is modeled by

$$\vec{\boldsymbol{M}}_I(x) = [M_x \quad M_y \quad 0]^T = M_I\left[cos\frac{2\pi x}{\lambda} \quad sin\frac{2\pi x}{\lambda} \quad 0\right]^T \tag{12}$$

The Eq. (12) clearly expresses that the magnetic orientation of the robot is a sine and cosine function. The direction of magnetic moments aligns as a waveform, and the distribution of magnetic moments is homogeneous along the body length, resulting in uniform magnetic strength. In Fig. 5a, once the I robot is actuated by the oscillating magnetic field, the magnetic moments embedded in its soft structure align with respect to the direction of the magnetic field, then induce the body deformation to become a wave, and since the magnetic field continuously oscillates, the body of the robot is continuously deformed, resulting in swimming forward with a lateral undulation. It is noticed that the deformation of the I robot is symmetric, and all of the specimen in the soft structure deforms equally. Note that wave length is 1, and $x \in l$.

3.2 Magnetic behavior of the II robot

The property of the II robot consists of non-uniform magnetic strength due to a triangular shape (1 mm × 6 mm × 80 μm), and uniform magnetic orientation which all directs to the same direction. As depicted in Table 3, the quantity of magnetic moments decreases along the body length, resulting in non-uniform strength across the whole structure according to the eq. (2). The position where the cross-sectional area is larger possesses a stronger magnetic strength. Thus, its magnetic property is modeled by

$$\vec{\boldsymbol{M}}_{II}(x) = [0 \quad M_y \quad 0]^T = M_{II}\,[0 \quad 1 \quad 0]^T \tag{13}$$

The Eq. (13) expresses that the magnetic strength of the II robot is a function of a position along length $\boldsymbol{l}$, and the magnetic moments are represented by the identity matrix 1, which all directs to the y direction. Under this property, once the robot is actuated by the oscillating magnetic field, the largest specimen containing the strongest magnetic strength firstly responds with the highest deformation degree, and heads to the direction of magnetic field. Other specimens containing lower magnetic strength subsequently respond. Thus, since the magnetic field oscillates, the robot behaves as if sweeping the body with respect to the direction of the oscillation, and this aspect makes the robot propel forwardly as shown in Fig. 5b.

3.3 Magnetic behavior of the III robot

The property of the III robot consists of non-uniform magnetic strength and non-uniform magnetic orientation. Similar to the II robot, the triangular shape provides an unequal quantity of magnetic moments in each cross-sectional area across the body length. As obvious, the magnetic orientation of the III

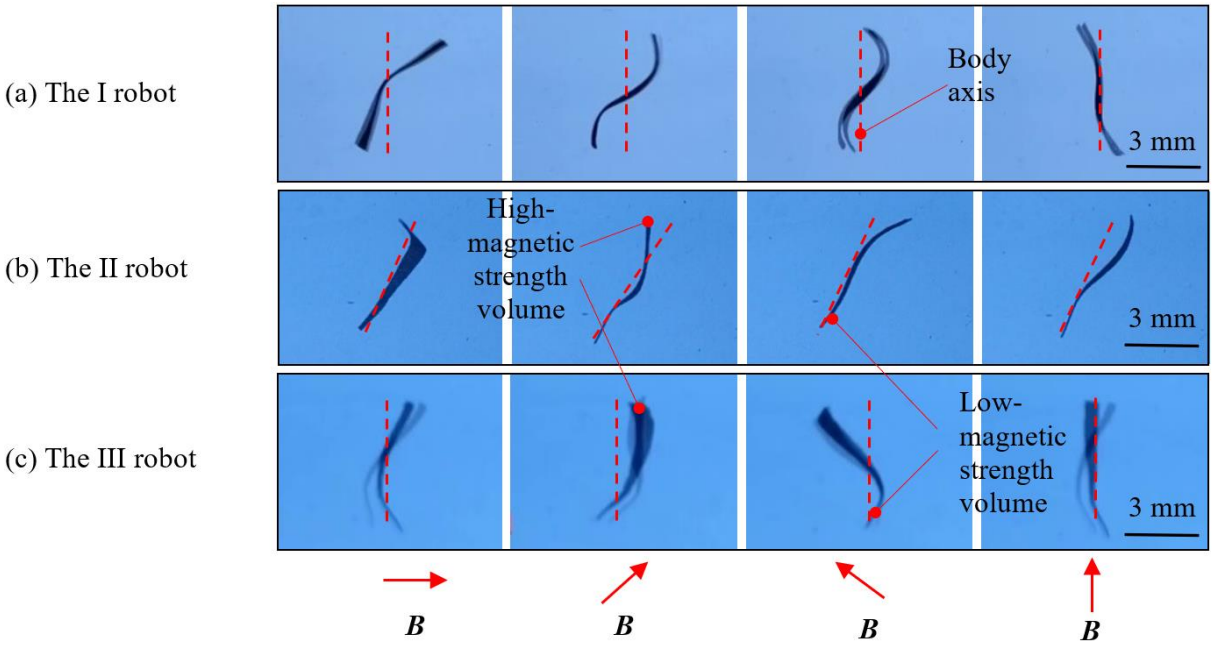

Fig. 5 Swimming behavior of three robots with distinguish magnetic property. (a) The I robot symmetrically deforms as a wave. (b) The II robot sweeps at the specimen of high magnetic strength. (c) The III robot propagates a body wave along the body length. The B represents the oscillating magnetic field, and the red arrow defines the direction of magnetic field.

robot is similar to the I robot which is in the sine form, representing non-uniformity of magnetic orientation. Thus, its magnetic property is modeled by

$$\overrightarrow{\boldsymbol{M}}_{III}(x) = [M_x \quad M_y \quad 0]^T = M_{III}\left[cos\frac{2\pi x}{\lambda} \quad sin\frac{2\pi x}{\lambda} \quad 0\right]^T \tag{14}$$

The Eq. (14) explicitly expresses that both magnetic orientation and strength are a function of the body length. The magnetic response of the III robot is the same as the I robot in case of magnetic orientation as a waveform, and to the II robot in case of deformation degree. Thus, once the III robot is actuated by the oscillating magnetic field, magnetic moments embedded in the soft structure induce the deformable body to become a waveform, but the deformation degree of each specimen of the soft structure is unequal. The largest specimen firstly responds with the highest deformation degree, and other specimens containing lower magnetic strength subsequently respond. Since the magnetic field continuously oscillates, these aspects induce the whole soft body of the robot to propagate as if a body is waving, resulting in lateral undulation, as depicted in Fig. 5c. Note that wave length is 1, and $x \in l$.

3.4 Comparison in Swimming Behavior and Performance

According to Fig. 5 and the supplementary video, when all robots (I, II, III) are under the oscillating magnetic field, they transform their deformable structure into a specific shape. The deformation pattern of the robots directly relates to the profile of magnetization, which can be programmed upon demands. For example, the sine profile makes the robot transform from a flat shape into a wave-liked shape. The continuous deformation of the robot leads to the asymmetric body deformation, and it is applied as a motor-less mechanism for swimming. The role of magnetic strength defined by the quantity of magnetic moments in the robot structure influences the degree of magnetic response of the robot to external magnetic actuation. If magnetic strength is stronger, the magnetic response is faster and the responsive degree is higher. If magnetic strength is weaker, slower response and a lower responsive degree. According to the Eqs. (10) and (11), amplitude (responsive degree) and velocity (fast degree) of a specimen in the robot structure are directly proportional to magnetization (quantity of magnetic moments) at that specimen. Interestingly, in the case of the III robot profiled by sine function, both high and low magnetic strength are combined in one single soft structure, as called non-uniform magnetic strength. The magnetic response of the entire body is sequentially from the high to low magnetic strength because the high magnetic strength is more attractive to magnetic actuation. As apparent, wave propagation then proceeds from the high to low magnetic strength volume. Additionally, the III robot shows high maneuverability. The rotating magnetic field can drive the robot to swim curvilinearly in along clockwise or counter-clockwise direction.

On the other hand, for the I robot, with the same sine wave profile, magnetic strength is uniform all across the structure. All specimens across the structure respond to the magnetic field equally, and the whole structure transforms into a waveform. In the case of the II robot which contains non-

uniform magnetic strength and one-direction of magnetic moments, it responds to magnetic field unequally. As obvious, the largest area is highly active to the magnetic field, and sweeps along the oscillating direction of the magnetic field, resulting in swimming.

Experiments are set up to investigate the swimming performance of three robots by placing them in a viscous fluid to simulate biological fluid conditions, and afterward, oscillating magnetic field with three magnitudes (5 mT, 10 mT, and 15 mT) and fifteen frequencies (from 1 to 15 Hz) is operated to drive the robots to laterally undulate or swim along the 10-cm straight path over the measured time. Due to the Electromagnetic Actuation System having a large homogeneous magnetic field, magnetic torque is then precise and reliable. In Fig. 6, swimming velocity is plotted against fifteen frequency numbers of the oscillating magnetic field, which is separated into three graphs according to three magnitudes of the actuating magnetic field. The results clearly report that swimming velocity tends to increase by an increase of the gaining oscillation frequency. The III robot swims fastest at all magnitudes and frequencies. All of the robots have the step-out point at 13 Hz. At this point, the robots lost in magnetic synchronization to the magnetic control, resulting in a velocity decrease. However, the swimming velocity of the II robot does not drop as fast as others because its magnetic orientation points toward only one direction. Its magnetic synchronization is a much simpler and faster response, and it still keeps swimming better than others even after reaching the step-out point. On the other hand, the I and III robots are profiled with the sine-curve magnetic orientation. Magnetic alignment of them is definitely much slower. That is why the I robot has no exceptional potential when compared to others, but in the case of the II robot, having non-uniform magnetic strength can compensate for the complicated alignment interestingly. Additionally, apart from the II robot, it shows the least loss in synchronization. After the step-out point at 13 Hz, it tends to keep a better swimming performance.

As apparent, the III robot is not only the best swimmer, but it can also be operated at the low power of the lowest actuating magnetic field; 5 mT. It keeps better control and performance than others at all ranges of frequency, whereas the others cannot swim due to a lost in magnetic synchronization at the low power.

3.5 Result & discussion

There are several preparations to avoid errors in data collection during the experiments. One of them is about the velocity data of the robots to make comparison plots. Since the robots are in millimeters, to precisely measure swimming velocity, the object tracking technique is applied to localize the coordinate of the present position of the robots via a real-time image captured by the camera mounted on the top of the Electromagnetic Actuation System. Another is to define the magnetic orientation of magnetic moments precisely. Before the magnetizing process, all robots are placed inside a shape guider to form a desired orientation. The guider is then printed with the high-resolution 3D printer. Another is magnetic field generation. The robots in this work are designed to operate in a fluidic environment, so the ability to move in fluid or swimming is crucial. Under this condition, pure magnetic torque is generated within a large homogeneous region of the magnetic field of the Electromagnetic Actuation System.

According to the experimental results, either magnetic orientation or strength or both of them can be applied as a swimming mechanism of the robots, but they have pros and cons or strong and weak points differently, which depends on the applications and tasks of the robot. For example, as stated by Purcell,[17] an asymmetric movement of microorganisms is a key success to swim in biological fluid. Although non-uniform orientation is a cause of the controllable body deformation for swimming, this technique would be viable for the robot larger than 500 μm due to the lack of the shape guider's dimension as well as precision of the magnetization profile. On the other hand, if the robot's size is down to micrometers or less, programming non-uniform orientation on the guider would be more complicated and difficult. Instead, the use of non-uniform strength is an alternative approach. Minimal control of the magnetic field can make the robot propel, as shown in the II robot. However, with the combination of non-uniformity in both aspects, the III robot shows the fastest swimming at all control parameters because there are two mechanisms supportive of each other. As known, high-strength specimens have a faster response to magnetic torque than low-strength specimens, but non-uniform orientation based on sine wave assists the low-strength specimens to deform the structure, and this feature enhances its performance. On the other hand, as obvious in the II robot, its low specimen which contains uniform orientation cannot respond to magnetic actuation under the same control parameter. In short, the dimension of the robot is the most crucial condition to indicate a proper type of magnetic property. Minorly, fluidic condition is another concern parameter that influences the form of magnetic orientation.

The fabrication process in this work allows additional elements to empower the soft milli-robot for further biomedical applications. In particular, we have a purpose to utilize the magnetic compliance of the robot for locomotion and to trigger embedded functions to treat abnormality, such as controllable drug release, *etc*. Another issue would be the partial biocompatibility of the robots, even though the results of this work report the reliability of the use of the robot in terms of performance and behavior. Biocompatible polymers (*e.g.*, PEG, hydrogel) can be used to wrap the robot. Another would be about how to visualize and track the robot inside the blind area or a living body where users cannot see the robot with bare eyes. There are two possible solutions, *e.g.*, the Ultrasound imaging to detect the robot, or the Photoacoustic (PA) imaging to visualize the robot as a contrast agent. As depicted in Fig. 7a, once the robot is placed within a blind area, the ultrasound imaging clearly visualizes it. Moreover, gold

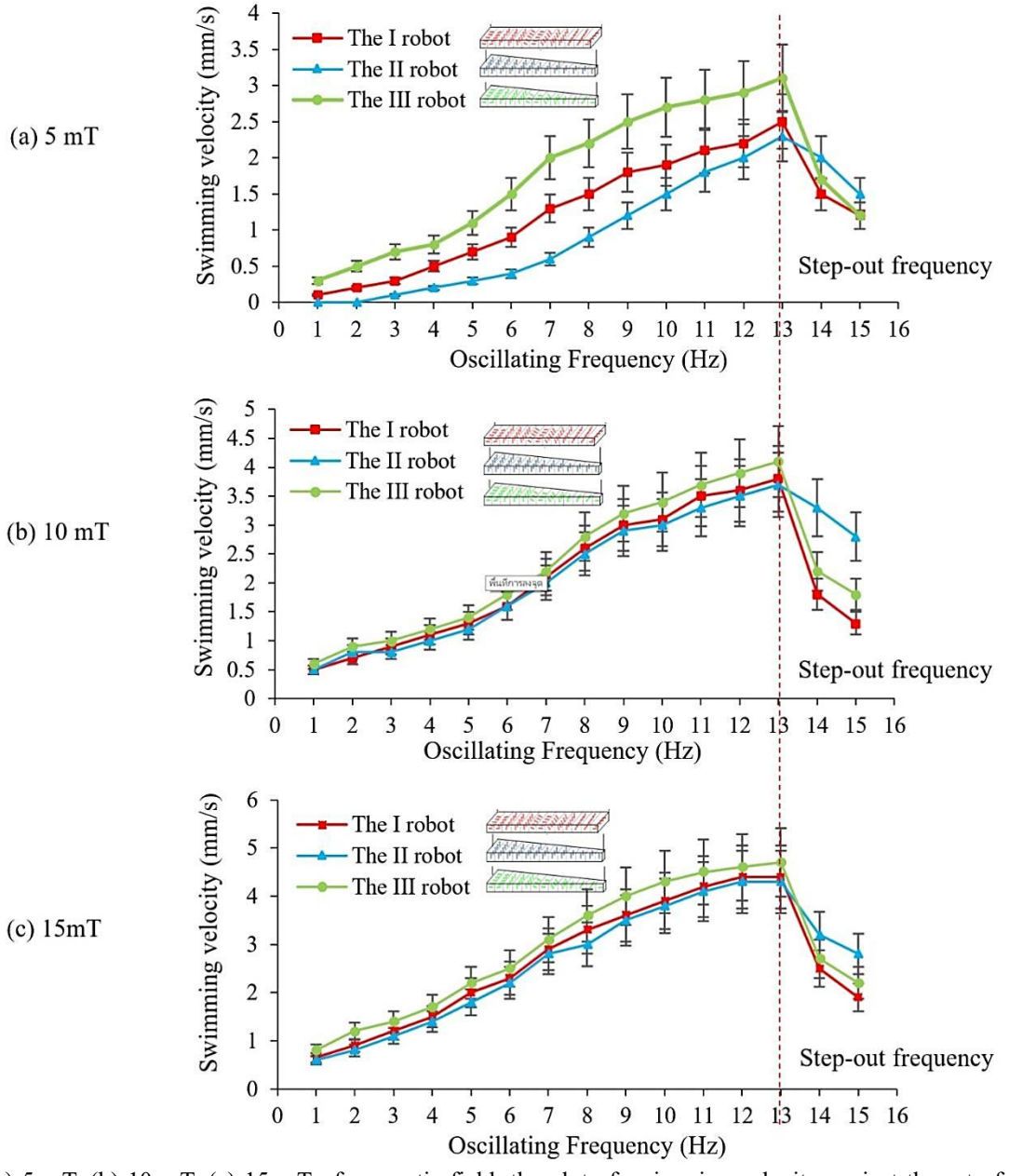

Fig. 6 Under (a) 5 mT, (b) 10 mT, (c) 15 mT of magnetic field, the plot of swimming velocity against the set of the oscillating frequency (ranged from 1 to 15 Hz). The robots all swim faster with the increase of the actuating frequency, and drops after reaching the step-out point at 13 Hz**.**

nanorods (AuNRs) are deposited into the mixture during the fabrication process detailed in Fig. 2A. After finishing, the AuNRs@mangetic soft milli-robot is placed inside the black and blind area. The Photoacoustic (PA) imaging machine (Vevo LAZR-X Fujifilm Visual Sonics Inc.) can detect the robot by using the 715 nm excitation wavelength and 40 Hz frequency, as depicted in Fig. 7b. At the 9-mm distance from the machine probe, the robot's head is clearly observed during positioning in the testing reservoir. The result clearly reports that both the ultrasound and PA techniques can be applied to visualize the robot. This approach would facilitate in life promisingly.

Although this work presents the robot on a millimeter scale and analyzes the pros and cons of each property of the robot, there are some interesting discussions about the swimming behaviors of the scaled-up or down robot. If the conditions of the fluidic environment and input parameters are not changed, in case of the scaling up, the robot still keeps the swimming behaviors (*e.g.* stoke, deformation characteristics, *etc*.) the same as the present scale, but the magnetic field to control it might need less due to the existence of higher magnetization magnitude of the robot, and the swimming velocity in unit of body length per second would be higher according to the larger scale. It would empower inertia force, leading to a high Reynold number swimmer. On the other hand, in case of the scaling down, the robot would keep the swimming behavior the same as the present scale as well, but the magnetic field needs much higher to actuate the robot, and it would swim

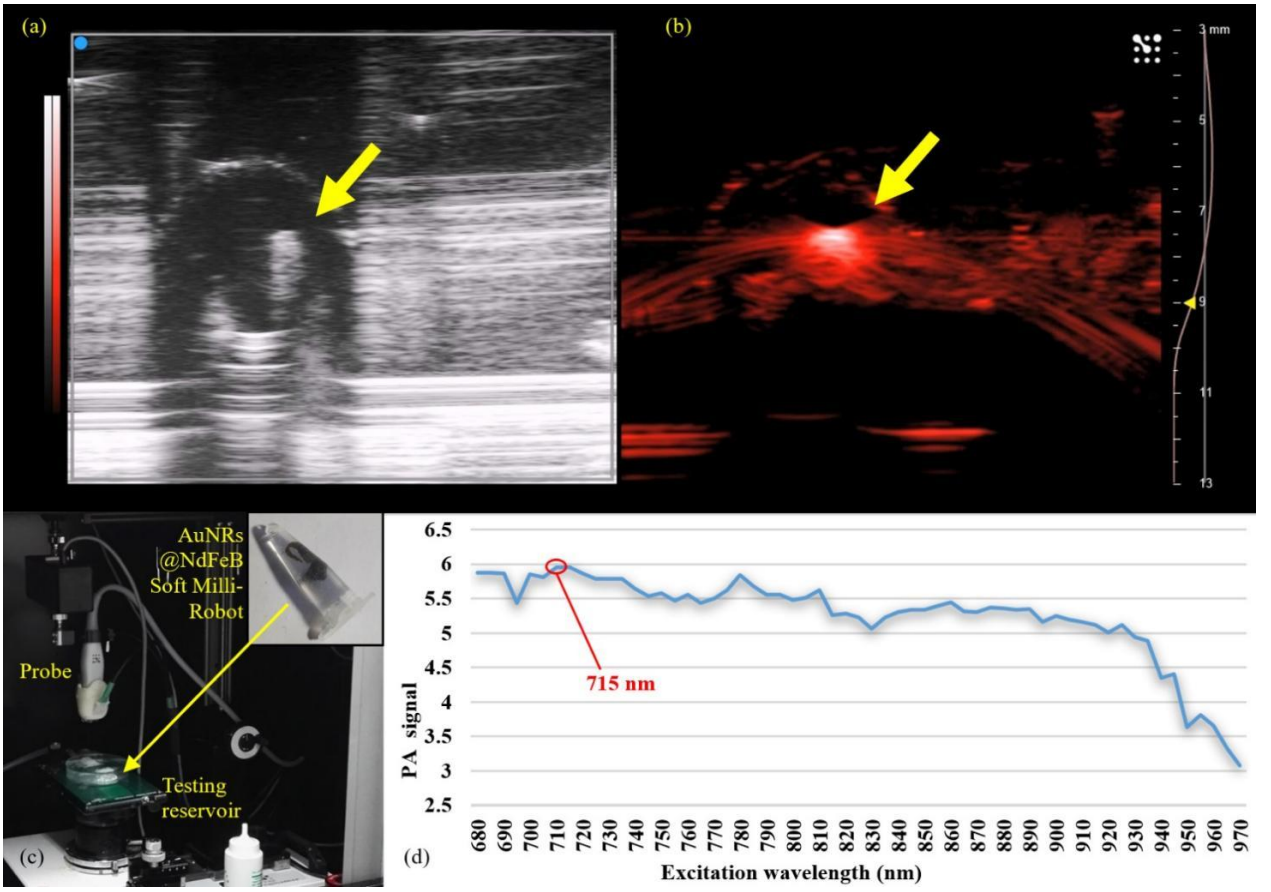

Fig. 7 Observation on gold nanorods-powered magnetic soft milli-robot (AuNRs:NdFeB:SLR with 0.5:1:1 ratio) in blind region by using Photoacoustic (PA) imaging machine. (a) Ultrasound image. The left grayscale and red-scale legend define the contrast display of ultrasound and PA mode in the machine settings, which are adjustable to visualize the robot's image clarity within the testing reservoir. (b) PA image (715 nm of excitation wavelength and 40 Hz frequency). The right scale bar displays the focal zone indicator used to observe the focused position of the robot in the testing reservoir, and the robot's head is at the 9-mm distance away from the probe. (c) Setup scheme in the PA machine. (d) the plot reports the response of the robot to different excitation wavelengths, and the 715 nm reports the best response by the highest PA signal (dimensionless).

slower because the body deformation cannot exert swimming force or thrust as much enough against viscous force, same to the present scale. Moreover, both cases can be alternatively explained by the Eq. 11 of the theoretical concept. The speed of the local specimen of the whole robot volume is proportional to the magnetic response of the robot in terms of magnetization profile to the actuating magnetic field. The higher the speed, the stronger the swimming force.

As obvious, the use of even minimal control of the magnetic field can manipulate the robot to perform unlimited structural changes, leading to swimming in fluid effectively. Once the robot is operated inside life for therapy, targeted drug delivery is advanced in potential through real-time controllable motion and trigger. This aspect advantages the adaptability of the robot to unpredictable conditions of life. Magnetic field, as known, contributes the great results in Medicines, such as MRI scanners. It is harmful to tissues and penetrates deep into organs.

4. Conclusions

Small-scaled robots are a part of medical robots, and they can access inside a living body to perform therapy and treatment due to their tiny size, controllability, and manoeuvrability within biological fluids. In the research of biomimetic robots, fish-like swimming adopting a flexible body is confirmed as one of the best in-fluid locomotion. If the size of the robot is down to a millimeter or less, a lack of a proper driving mechanism that is smaller than the robots is a big issue. Alternative power sources (*e.g.* magnetic field, light, sound) to remotely power the robot are then a solution to the problem promisingly. As known, several medical devices (*e.g.*, MRI, MPI) all utilize magnetic fields to image inside a living body. Nowadays, there is no doubt in their potential, including riskless and harmless to tissue and organs. As well, it is untethered, controllable, and penetrable into blind areas. Since the demand to access inside a living body for medical applications is size, scaling down the robot to a sub-millimeter or less is a solution. Yet, in the current technology, neither the battery nor the mechanism is smaller than a millimeter to set up within the structure of the small-scaled robot. The magnetic field is employed to power the robot through the magnetic response of the active elements embedded within the robot's

body. Remotely magnetic manipulation is an effective and non-harmful technique to control small-scaled robots as a medical device to deal with biomedical applications.[19] In this work, a flexible structure of soft material is combined with magnetic active micro-elements to fabricate a soft swimming milli-robot for medical application. This concept enables the wireless power of the external magnetic field to control the robots' locomotion as well as functional triggering. Magnetic moments embedded in the soft structure align with the actuating magnetic field, leading to controllable body deformation and swimming effectively. However, based on the theoretical concept of magnetism, magnetic moments as a vector play important roles in swimming behavior and performance consisting of orientation and strength. Three soft swimming milli-robots with distinguished magnetic properties are investigated. Finally, the experimental results report that the quantity and orientation of magnetic moments in the soft structure function swimming behavior and performance of the robot differently. Either or both of them can be employed as a motion mechanism of the soft swimming milli-robots. Some tasks operated in fluidic flow might need the II robot type because its maneuverability is better than others. some tasks are operated at high frequency, where the II robot is much more appropriate. The contribution of this study is wide-opening and promising for the robots to serve multi-purposes towards biomedical applications.

Acknowledgements

This work is supported by the Thammasat University Research Fund No. TUFT77/2567, the Thammasat Postdoctoral Fellowship No. TUPD11/2567, the Thailand Science Research and Innovation Fundamental Fund fiscal year 2023, and the National Research Council of Thailand (NRCT) and Thammasat University No. N42A671063.

Conflict of Interest

There is no conflict of interest.

Supporting Information

es1135_SI as the supplementary video shows the swimming behaviors of three robots.

References

[1] B. J. Nelson, I. K. Kaliakatsos, J. J. Abbott, Microrobots for minimally invasive medicine, *Annual Review of Biomedical Engineering*, 2010, **12**, 55-85, doi: 10.1146/annurev-bioeng-010510-103409.

[2] L. Manamanchaiyaporn, T. Xu, X. Wu, An optimal design of an electromagnetic actuation system towards a large homogeneous magnetic field and accessible workspace for magnetic manipulation, *Energies*, 2020, **13**, 911, doi: 10.3390/en13040911.

[3] X. Tang, L. Manamanchaiyaporn, Magnetic-powered swimming soft-milli robot towards non-invasive applications, 2022 8th International Conference on Control, Decision and Information Technologies (CoDIT). Istanbul, Turkey. IEEE, 2022.

[4] L. Manamanchaiyaporn, T. Xu, X. Wu, Magnetic soft robot with the triangular head–tail morphology inspired by lateral undulation, *IEEE/ASME Transactions on Mechatronics*, 2020, **25**, 2688-2699, doi: 10.1109/TMECH.2020.2988718.

[5] S. Palagi, P. Fischer, Bioinspired microrobots, *Nature Reviews Materials*, 2018, **3**, 113-124, doi: 10.1038/s41578-018-0016-9.

[6] L. Zhang, J. J. Abbott, L. Dong, B. E. Kratochvil, D. Bell, B. J. Nelson, Artificial bacterial flagella: fabrication and magnetic control, *Applied Physics Letters*, 2009, **94**, 064107, doi: 10.1063/1.3079655.

[7] H.-W. Huang, M. S. Sakar, A. J. Petruska, S. Pané, B. J. Nelson, Soft micromachines with programmable motility and morphology, *Nature Communications*, 2016, **7**, 12263, doi: 10.1038/ncomms12263.

[8] E. Diller, J. Zhuang, G. Zhan Lum, M. R. Edwards, M. Sitti, Continuously distributed magnetization profile for millimeter-scale elastomeric undulatory swimming, *Applied Physics Letters*, 2014, **104**, 174101, doi: 10.1063/1.4874306.

[9] G. Z. Lum, Z. Ye, X. Dong, H. Marvi, O. Erin, W. Hu, M. Sitti, Shape-programmable magnetic soft matter, *Proceedings of the National Academy of Sciences of the United States of America*, 2016, **113**, 6007–6015, doi: 10.1073/pnas.1608193113.

[10] W. Hu, G. Z. Lum, M. Mastrangeli, M. Sitti, Small-scale soft-bodied robot with multimodal locomotion, *Nature*, 2018, **554**, 81-85, doi: 10.1038/nature25443.

[11] M. Cianchetti, C. Laschi, A. Menciassi, P. Dario, Biomedical applications of soft robotics, *Nature Reviews Materials*, 2018, **3**, 143-153, doi: 10.1038/s41578-018-0022-y.

[12] M. Sitti, Miniature soft robots—road to the clinic, *Nature Reviews Materials*, 2018, **3**, 74-75, doi: 10.1038/s41578-018-0001-3.

[13] L. Manamanchaiyaporn, X. Tang, Y. Zheng, X. Yan, Molecular transport of a magnetic nanoparticle swarm towards thrombolytic therapy, *IEEE Robotics and Automation Letters*, 2021, **6**, 5605-5612, doi: 10.1109/LRA.2021.3068978.

[14] E. Gultepe, J. S. Randhawa, S. Kadam, S. Yamanaka, F. M. Selaru, E. J. Shin, A. N. Kalloo, D. H. Gracias, Biopsy with thermally-responsive untethered microtools, *Advanced Materials*, 2013, **25**, 514-519, doi: 10.1002/adma.201203348.

[15] W. Zhu, J. Li, Y. J. Leong, I. Rozen, X. Qu, R. Dong, Z. Wu, W. Gao, P. H. Chung, J. Wang, S. Chen, 3D-printed artificial microfish, *Advanced Materials*, 2015, **27**, 4411-4417, doi: 10.1002/adma.201501372.

[16] C. W. de Silva, S. Xiao, M. Li, C. N. de Silva, Telemedicine–remote sensory interaction with patients for medical evaluation and diagnosis, *Control and Intelligent Systems*, 2013, **41**, 1-2, doi: 10.2316/journal.201.2013.4.201-2536.

[17] E. M. Purcell, Life at low Reynolds number, *American Journal of Physics*, 1977, **45**, 3-11, doi: 10.1119/1.10903.

[18] N. A. Spaldin, Magnetic Materials Fundamentals and Applications,2nd edition, Cambridge University Press, USA, 2010.

[19] L. Manamanchaiyaporn, T. Xu, X. Wu, Electromechanical

energy-based 3D-controllable motion of small matter toward tiny machines, *Energies*, 2024, **17**, 1155, doi: 10.3390/en17051155.